Exploring Antarctic Lidar Measurements to Investigate Gravity Wave Energy Dynamics using New Data Processing Techniques

Jackson Jandreau and Xinzhao Chu,

CIRES and Aerospace Engineering, University of Colorado Boulder

Abstract and Background

Lidar Observations of gravity waves have been made over McMurdo Station, Antarctica near-continuously since 2010 [1, 2]. Lidar can measure waves in a wide spectra from diurnal tides to turbulence, enabling a range of studies. These gravity waves are persistent, appearing in nearly every observation, extending from the lower stratosphere to the mesosphere-lower-thermosphere (MLT).

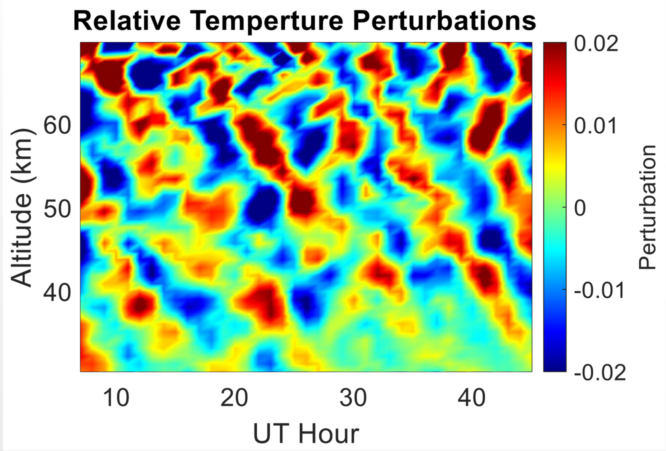

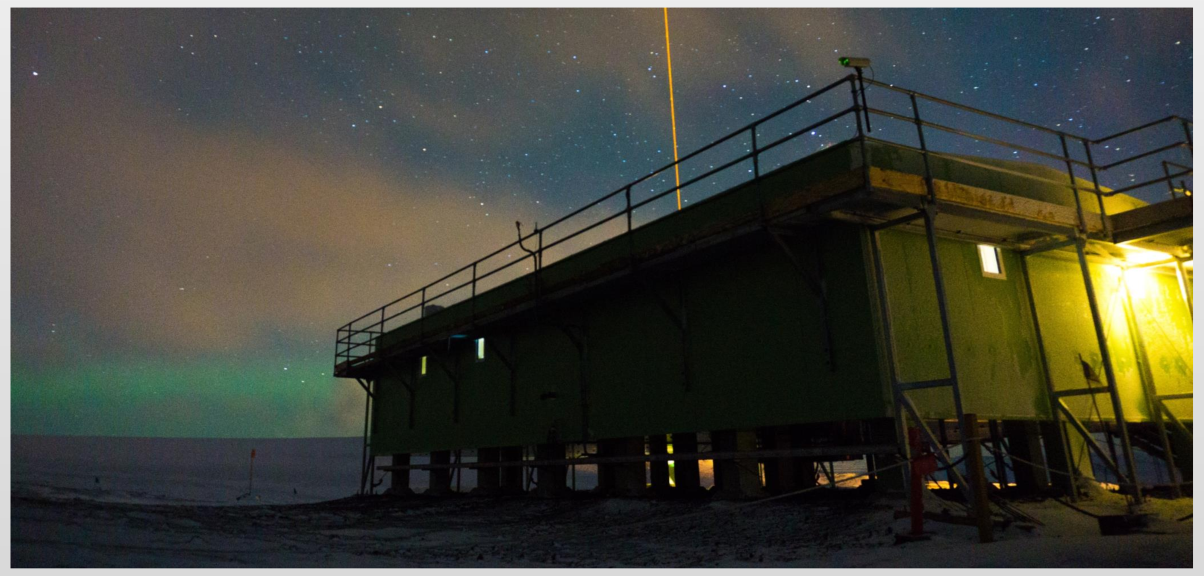

This variability study is enabled by the 10-yr dataset and searches for trends and relations within both wave energy measurements and the spectral components of these waves. Variability is found in all of these factors, but further study is needed to confirm and expand the spectral properties.

Above: Image of the McMurdo Observatory **Above-right:** Contour of gravity wave perturbations

Goals

- **Determine baseline "climatological" measurements** for wave energy and spectra
- **Identify variability** (or lack of it) in a quantifiable manner and **trace its sources**
- **Assess vertical coupling**: *"How does the lower atmosphere affect the upper?"*
- **Observe/confirm gravity wave interactions** with each other and with external factors

Results

Potential energy density (Epm) characterizes the strength of wave perturbations and grows exponentially with altitude alongside decreasing background density. The newly developed Interleaved Method [3] was used for these calculations, described briefly below. The use of this method enabled reliable winter measurements up to 70 km enhancing study of the gap region between the Rayleigh and MLT data.

These spectra represent the 10-yr average of monthly m-spectra found by Hanning-windowing and an autoregressive pre-whitening/post-coloring (PWPC) [4] in order to minimize leakage of low-wavenumber power. Spectral power in this case was calculated by the equations below. These spectra are considered **preliminary results**, as the analysis and PWPC process need additional fine-tuning.

The Interleaved Method:

Directly calculated Epm in inherently biased by the noise seen in Eq. 2. This complicates the use of Epm and necessitates a correction method. The Interleaved Method was recently developed to handle this problem.

The sample is split into two independent temperature perturbation samples by grouping alternating photon counts. This emulates two lidars making measurements on the same atmosphere parcel.

This generates two samples whose wave component is correlated, and noise components are not. Upon calculating a covariance from these samples as in Eq. 3, the averaging causes the noise components approach zero, systematically removing any bias from the variance.

This covariance can then be used in lieu of variance in Eq. 1 to calculate a bias-free Epm. Jandreau and Chu, 2022 explored this and other bias removal methods and found the Interleaved Method best for this case.

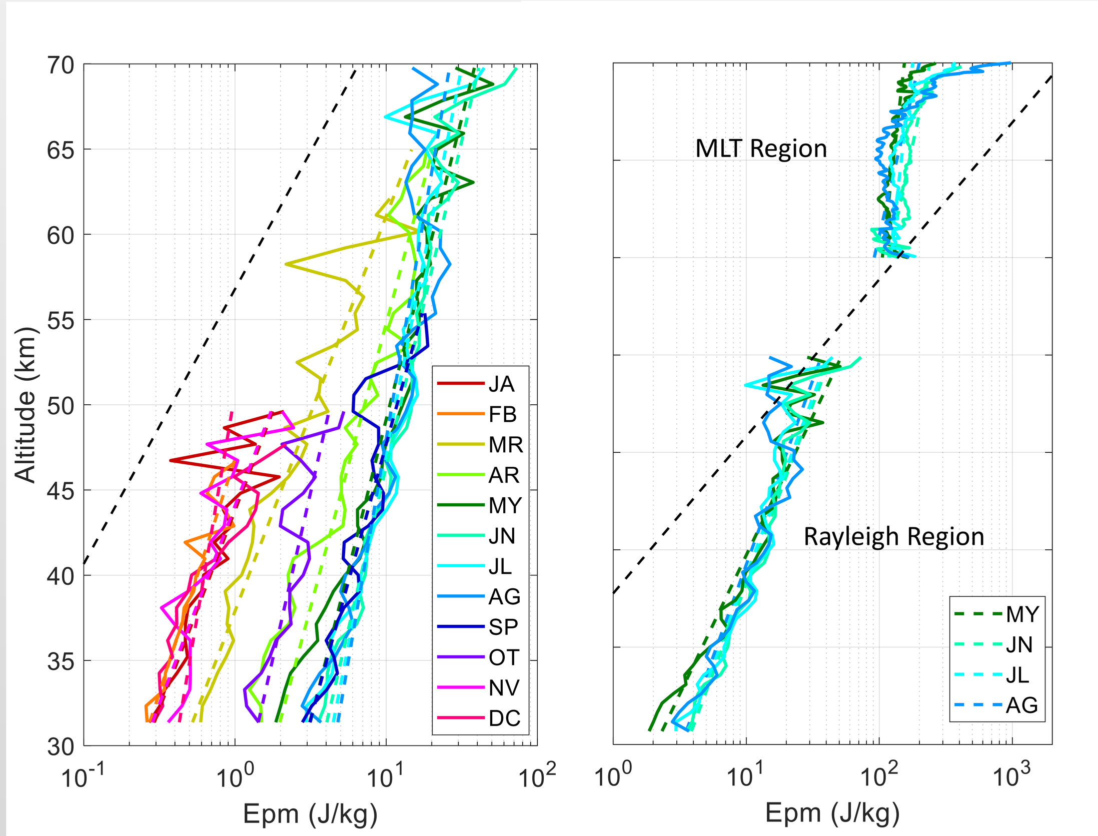

Above: Epm plots from 2011-2020 representing each month

1. $Epm(z) = \frac{1}{2}\frac{g^2}{N^2}Var(T_{relative})$

2. $Var[T'_{total}(z)] = \overline{[T'_{total}(z)]^2} = \overline{(T' + \Delta T)^2} = \overline{(T')^2} + \overline{(\Delta T)^2} + \overline{(2T'\Delta T)}$

3. $Cov_{Wave} = \overline{T'_A T'_B} = \overline{T'_A T'_B + T'_A \Delta T_B + T'_B \Delta T_A + \Delta T_A \Delta T_B} =$

Pre-whitening (k-th order autoregressive)

$$w(z) = x(z) - \sum_{n=1}^{k} \phi_n x(z-n)$$

Periodogram Calculation

$$PSD(\omega) = \frac{2 * \delta t}{N}|F(\omega)|^2$$

Post-coloring

$$PSD(\omega) = \frac{PSD(\omega)}{\left|1 + \sum_{n=1}^{k} \phi_n e^{-i\omega n \delta z}\right|}$$

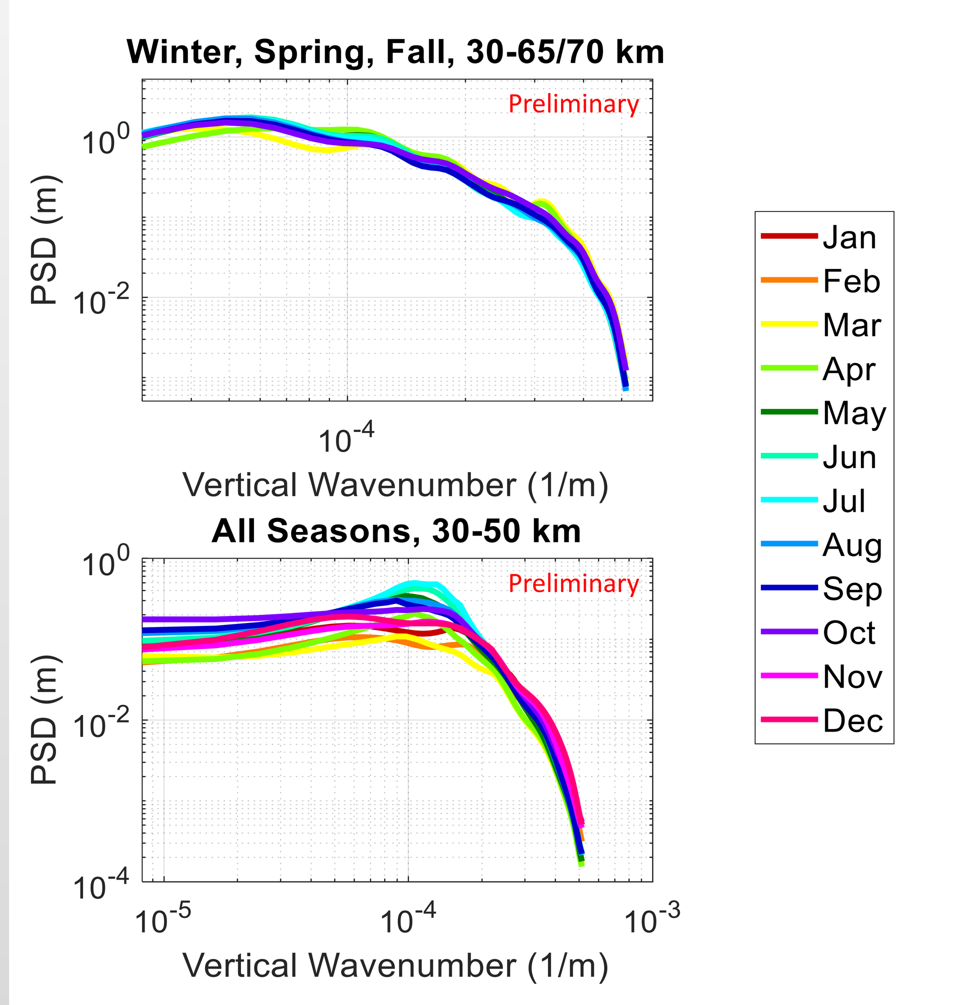

Above: Spectral plots showing statistical m power distribution

Data

This data has been collected over the 10-yr McMurdo Lidar campaign. The data used here comes from a Fe Boltzmann lidar which measures the stratosphere and mesosphere using Rayleigh scattering, and the MLT using Fe resonance fluorescence.

This data is processed according to its SNR; higher SNR seasons span a wider range. Data is screened according to its uncertainty level (>2.5% is removed).

May, Jun, Jul, Aug	30-70 km
Nov, Dec, Jan, Feb	30-50 km
Mar, Apr, Sep, Oct	30-65 km

The wave perturbations were found by removing the temporal background and spectrally filtering to the ranges below.

Rayleigh Region

Wavelength (km): 2-30

Period (hr): 2-11

MLT Region

Wavelength (km): 1-30

Period (hr): 0.5-11

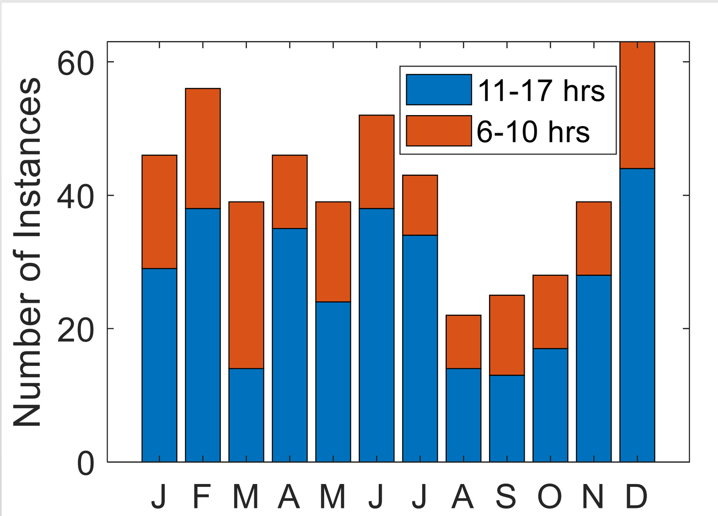

Right: Histogram of data length and distribution

Discussion of Variability

Due to the low-altitude of summer data, this variability study was limited to 30-50 km in order to compare all months. The spectral variation curves were smoothed by 6-months to highlight trends

Characteristic wavenumber is where the slope of the spectrum begins to change to a steeper slope.

The slope is determined by fitting a line for the equation $\log_{10}(y) = m * \log_{10}(x) + b$ to the portion of the spectrum from the characteristic wavenumber to the high end of the spectrum.

For comparison, 30-50 km Epm means and their fits (diurnal + semidiurnal) are shown, processed with the Interleaved Method. This shows a known seasonal asymmetry and year-to-year variation [5, 6].

The year-to-year variation is much clearer in Epm than the spectral properties. The m-slope does not show much variation from year-to-year yet shows a weak seasonal variation. The characteristic wavenumber shows a much stronger seasonal variation, and shows minimal year-to-year variation, with exception of 2019-2020 which appear to show a reduction in variation amplitude.

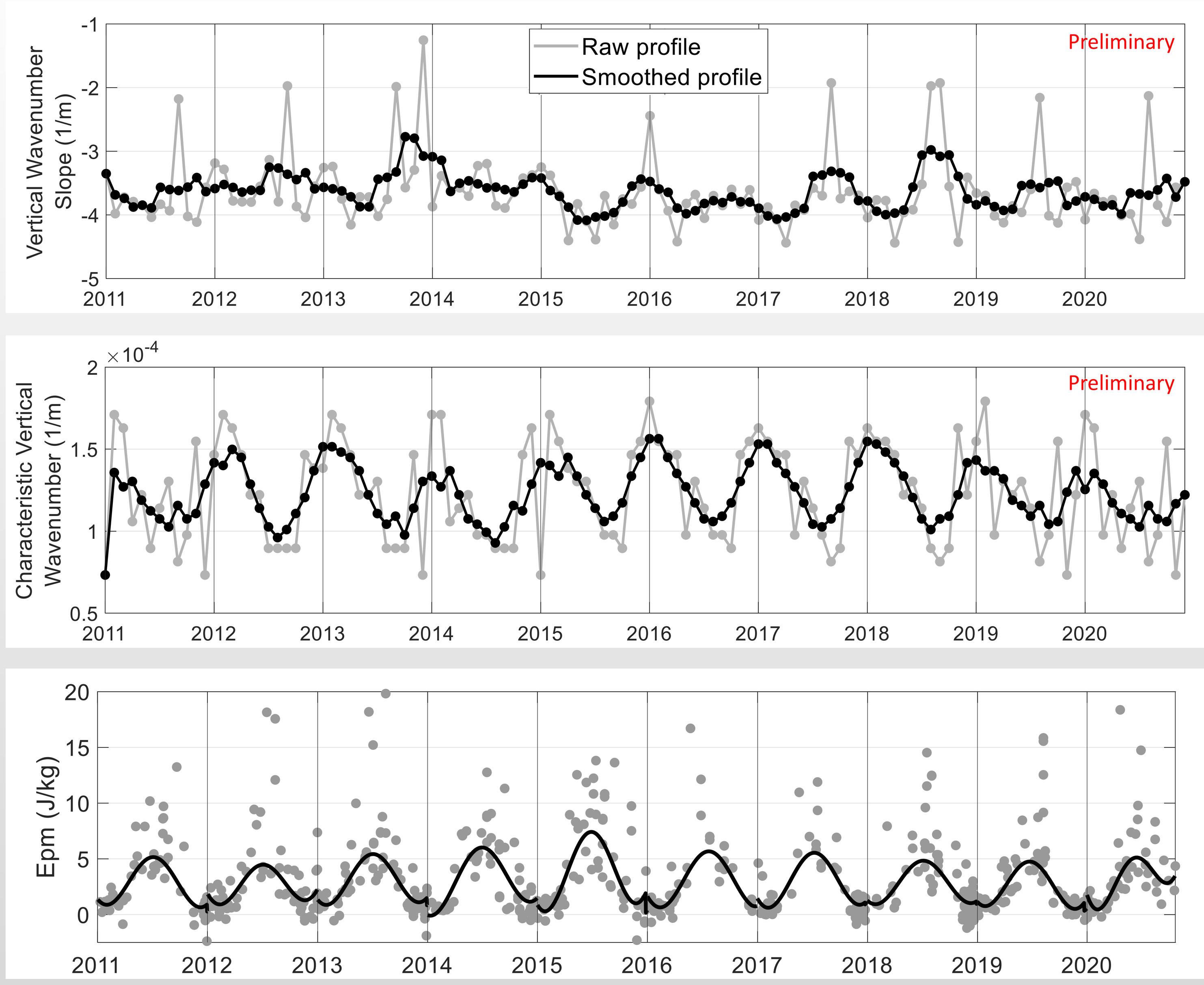

Top: Vertical wavenumbers **Middle:** Characteristic Vertical wavenumbers **Bottom: Annual** Epm variation

Conclusions

There appears to be minor seasonal variation in the spectral properties, but no major year-to-year variability is found. This is a preliminary presentation of an ongoing work to characterize McMurdo's wave energies and spectra, further study will be needed to confirm these trends and analyze their development over different altitude ranges.

Future efforts will largely focus on improving spectral calculations, applying the process to ω-spectra, and performing these calculations on MLT gravity waves. A major step following these will be to analyze the variations to determine their causes and driving factors.

References

1. Chu, X., W. Huang, W. Fong, Z. Yu, Z. Wang, J. A. Smith, and C. S. Gardner, First lidar observations of polar mesospheric clouds and Fe temperatures at McMurdo (77.8°S, 166.7°E), Antarctica, *GRL, 38,* L16810, doi: 10.1029/2011GL048373, 2011.
2. Chu, X., Z. Yu, C. S. Gardner, C. Chen, and W. Fong (2011), Lidar observations of neutral Fe layers and fast gravity waves in the thermosphere (110-155 km) at McMurdo (77.8°S, 166.7°E), Antarctica, *GRL*., 38, L23807, doi: 10.1029/2011GL050016.
3. Jandreau, J., & X. Chu (2022). Comparison of Three Methodologies for Removal of Random-Noise-Induced Biases from Second-Order Statistical Parameters of Lidar and Radar Measurements. *Earth and Space Sci*., e2021EA002073, doi: https://doi.org/10.1029/2021EA002073
4. Chen, C., and X. Chu (2017), Two-dimensional Morlet wavelet transform and its application to wave recognition methodology .. from lidar observations in Antarctica, *J. of Atmos. and Solar-Terr. Phys.*, 162, 28-47, doi: 10.1016/j.jastp.2016.10.016.
5. Chu, X., J. Zhao, X. Lu, V. L. Harvey, R. M. Jones, C. Chen, W. Fong, Z. Yu, B. R. Roberts, and A. Dörnbrack (2018), Lidar observations of stratospheric gravity waves from 2011 to 2015 at McMurdo (77.84° S, 166.69° E), Antarctica: Part II. Potential energy densities, lognormal distributions, and seasonal variations, *JGR: Atmos*., 123, doi: 10.1029/2017JD027386.
6. Li, Zimu, X. Chu, V. L. Harvey, J. Jandreau, X. Lu, Z. Yu, J. Zhao, and W. Fong (2020), First Lidar Observations of Quasi-Biennial Oscillation-Induced Interannual Variations of Gravity Wave Potential Energy Density at McMurdo via a Modulation of the Antarctic Polar Vortex, *JGR: Atmospheres*, 125, e2020JD032866. https://doi.org/10.1029/2020JD032866